

peerRTF: Robust MVDR Beamforming Using Graph Convolutional Network

Daniel Levi, Amit Sofer and Sharon Gannot

Abstract—Accurate and reliable identification of the relative transfer functions (RTFs) between microphones with respect to a desired source is an essential component in the design of microphone array beamformers, specifically when applying the minimum variance distortionless response (MVDR) criterion. Since an accurate estimation of the RTF in a noisy and reverberant environment is a cumbersome task, we aim at leveraging prior knowledge of the acoustic enclosure to robustify the RTFs estimation by learning the RTF manifold. In this paper, we present a novel robust RTF identification method, tested and trained with real recordings, which relies on learning the RTF manifold using a graph convolutional network (GCN) to infer a robust representation of the RTFs in a confined area, and consequently enhance the beamformer’s performance.¹

Index Terms—robust MVDR beamformer, manifold learning, graph convolutional network

I. INTRODUCTION

Modern acoustic beamformers outperform conventional direction of arrival (DOA)-based beamformers due to their ability to consider the entire acoustic propagation path rather than only the direct path. The construction of these beamformers necessitates an estimate of the acoustic impulse responses (AIRs) relating the source and the microphones (or their corresponding acoustic transfer functions (ATFs)). Given that ATF estimation poses a blind problem, the approach in [1] suggests replacing the ATFs with the RTFs in the beamformer design.

The RTF is defined as the ratio between two ATFs. Specifically, it represents the ATF that relates the source to one microphone, normalized by the ATF that relates the source to a designated reference microphone. This definition encapsulates the relative acoustic relation between microphones in an array. It effectively captures the relative differences in how the sound propagates to different microphones, which is crucial for various acoustic signal processing tasks. Various RTF-based audio beamformers can be found in the literature, often yielding improved performance compared to DOA-based beamformers. While various algorithms for estimating RTFs can be found in the literature, such as those proposed in [1]–[5], they often face degradation in low signal-to-noise ratio (SNR) and high reverberation conditions.

¹The authors are with Bar-Ilan University, Israel. e-mail: {daniel.levil, amit.sofer, sharon.gannot}@biu.ac.il. The work was partially supported by grant #3-16416 from the Ministry of Science & Technology, Israel, and from the European Union’s Horizon 2020 Research and Innovation Programme, Grant Agreement No. 871245. Daniel Levi and Amit Sofer equally contributed to the paper. Project Page: <https://peertrf.github.io/> (including audio demonstration and link to code).

The literature extensively covers approaches to enhance beamforming robustness, commonly achieved through techniques like beam widening, as discussed in [6]–[11]. In this work, our approach focuses on improving the estimated RTF by leveraging a pre-learned set of RTFs utilizing a modern manifold technique.

Despite their intricate structure, it is demonstrated in [12] that the RTFs are primarily controlled by a limited set of parameters, such as the size and geometry of the room, the positions of the source and the microphones, and the (frequency-dependent) reflection coefficients of the walls. Consequently, acoustic paths exhibit low-dimensional geometric structures, commonly referred to as manifolds, and can, therefore, be analyzed using manifold learning (ML) methods. In a fixed room with a static microphone array location, the only degree of freedom is the source location, causing the RTF to vary only based on the speaker’s position. Consequently, RTFs from different locations lie on a manifold. By assembling a clean set of RTFs as a training dataset, we can explore the RTF manifold and derive a more robust estimate of the RTF from noisy recordings.

Several ML approaches, such as those proposed by [13]–[15], typically follow a standard framework. In this framework, manifold samples are initially represented as a graph. Subsequently, a low-dimensional representation (embedding) of the data is inferred, preserving its structure meaningfully. This representation effectively ‘flattens’ the original non-Euclidean structure of the manifold into an Euclidean space, simplifying subsequent analysis. Post-inference, an algorithm is applied to the low-dimensional embedding to accomplish the desired task.

The MVDR beamformer is a spatial filter designed to minimize the noise power in its output while preserving the desired source without distortion. There is accumulated evidence that justifies the use of the RTFs as the steering vector for calculating the MVDR weights [1], [16], [17]. In our research, we adopt this approach.

In recent years, geometric deep learning (GDL), a term describing techniques that extend deep neural models to non-Euclidean inputs like graphs and manifolds, has seen significant application in classification, segmentation, clustering, and recommendation tasks. Its adoption is more prevalent in fields like social sciences (e.g., analyzing social networks using graphs), chemistry (where molecules can be represented as graphs), biology (where bio-molecular interactions form graph structures), 3D point cloud ML, computer vision, and others. Those methods usually focus on classification, segmentation,

clustering, and recommendation tasks but not on regression tasks. Graph neural network (GNN), a specific type of GDL, specializes in learning representations from graph-structured data by effectively propagating information between interconnected nodes. A particular type of GNN is the GCN which is based on the principles of learning through shared-weights, similar to convolutional neural networks (CNNs) [18]–[23]. GCNs effectively leverage graph structures by performing convolution operations over the nodes and edges, allowing them to capture the local neighborhood information and aggregate features from adjacent nodes. This approach enables GCNs to learn meaningful representations of graph-structured data.

Previous efforts to learn the manifold of the RTFs have employed a graph representation, utilizing the Gaussian heat kernel to determine edge weights [24], [25]. Spectral graph theory is then applied to infer a low-dimensional embedding of the manifold in Euclidean space. The Euclidean distance between samples in this transformed space reflects the diffusion distance on the manifold surface. Subsequently, leveraging geometric harmonics, an algorithm is employed to extend the training data and estimate the RTF based on the acquired manifold and the noisy signals. This algorithm effectively projects the noisy RTF onto the learned manifold of potential RTFs, resulting in a more robust estimation of the RTF.

Recent advances demonstrate that GNNs naturally emerges in ML. Inspired by these trends, we aim to substitute the traditional ML techniques with methods relying on GNN, particularly on GCN. The conventional ML techniques involve flattening the non-Euclidean manifold into an Euclidean space. We will harness the power of GCN to learn the high dimensional RTF manifold and to infer a robust estimator of a RTF from noisy measurements thereof by leveraging the graph representation of the manifold.

Our contribution is twofold: 1) a novel robust RTF estimation algorithm that infers the RTF manifold using a GCN and leverages it to robustify the RTF estimation; 2) a comprehensive assessment of the proposed scheme and its performance advantages as compared with competing methods in various SNR levels and real-world acoustic scenarios. The remainder of this paper is organized as follows. In Sec. II, we formalize the problem. Section III describes the relations between ML and graphs and presents the GNN framework, and in particular, the GCN variant. Section IV explains a general robust beamforming approach, which includes the vanilla RTF estimation and RTF-based beamforming. Section V elaborates on our approach, in particular, the creation of the graph data, the architecture of our network, and the objective Functions. Section VI describes the experimental setup and presents the results together with an elaborated comparison with other competing methods. Section VII concludes the paper.

II. PROBLEM FORMULATION

An M -microphone array is positioned in a reverberant enclosure. We assume that the desired source location is confined to a known region. Examples of such environments include conference rooms, where the microphone array is

placed at a fixed location on the table, and speakers occupy designated positions around it. Similarly, in office setups, the microphone array is fixed on the desk or computer screen, with the speaker typically seated behind the desk. In a car, the microphone array is positioned at a fixed location at the visor, while the speaker occupies one of the seats.

Let $r_m(t), m = 0, \dots, M - 1$, denote the measured signal at the m th microphone:

$$r_m(t) = \{s * a_m\}(t) + v_m(t), \quad (1)$$

with $s(t)$ representing the desired speech signal, and $v_m(t)$ the contribution of all noise sources as captured by the m th microphone, $a_m(t)$ stands for the AIR from the source to the m th microphone at time t , and $*$ denotes the convolution operator. In scenarios where the speaker remains static, the AIR remains constant over time. The time-domain convolution in (1) can be approximated by multiplication in the short-time Fourier transform (STFT) domain. All M equations can then be written in a single vector form as:

$$\mathbf{r}(l, k) = s(l, k)\mathbf{a}(k) + \mathbf{v}(l, k). \quad (2)$$

Here, l and k represent the time-frame and frequency-bin indexes, respectively, with $l \in \{0, \dots, L - 1\}$ and $k \in \{0, \dots, K - 1\}$. The vector $\mathbf{a}(k) = [a_0(k), \dots, a_{M-1}(k)]^\top$, comprises all ATFs from the source to the microphone array. We define $a_{\text{ref}}(k)$ as the component of the vector $\mathbf{a}(k)$ that corresponds to the reference microphone. Equation (2) can also be reformulated as a function of $\tilde{s}(l, k) = s(l, k)a_{\text{ref}}(k)$, representing the source signal as captured by the reference microphone:

$$\mathbf{r}(l, k) = \tilde{s}(l, k)\mathbf{h}(k) + \mathbf{v}(l, k), \quad (3)$$

where $\mathbf{h}(k)$ is the vector of RTFs:

$$\mathbf{h}(k) \triangleq \frac{\mathbf{a}(k)}{a_{\text{ref}}(k)}. \quad (4)$$

Playing a precisely defined signal, such as a chirp or white noise, without any background noise, from different locations within the desired acoustic environment enables us to use standard methods for identifying the system. This process yields a collection of RTFs. We aim to glean insights into the RTF manifold using this ensemble of clean RTFs. This can be leveraged to enhance estimates of noisy RTFs from the same enclosure, thereby robustifying the beamformer's design.

III. MANIFOLD LEARNING & GRAPH NEURAL NETWORKS

A. Graphs in manifold learning

In manifold learning (ML) problems, the objective is to infer a low-dimensional representation of data originating from a high-dimensional space. All ML algorithms follow a standard blueprint. First, they generate a data representation by constructing a neighbor graph. Second, they compute a low-dimensional representation (embedding) of the data, preserving a specific aspect of the original manifold structure. For instance, locally linear embedding [14], Isomap [13], and

Laplacian eigenmaps [15] use different techniques. Variational autoencoder (VAE) [26] introduces a distribution at the embedding stage (the encoder output). Extensions, e.g., conditional VAEs [27] and adversarial autoencoders (AEs) [28] aim at structured data representation. The new embedding ‘flattens’ the original non-Euclidean structure of the manifold, making it more manageable. After inferring the representation, the last step is to use the manifold’s low-dimensional embedding in a task-dependent algorithm (classification, clustering, or regression).

ML has found various applications in audio, including localization [29]–[32] and speech enhancement [24], [25], [33]. In [25], the RTF manifold is initially represented by a graph, where the RTFs serve as graph nodes, and the edges’ weights are defined using the heat kernel function. A Markov process is established on the graph by constructing a transition matrix representing the manifold diffusion process. Subsequently, leveraging spectral graph theory, a low-dimensional embedding of the dataset in Euclidean space is derived. In this space, the Euclidean distance between samples reflects the diffusion distance across the high-dimensional manifold surface. Once this low-dimensional embedding is obtained, geometric harmonics [34], a method extending low-dimensional embeddings to new data points, is employed to create a supervised RTF identification estimator. In [33], a VAE-based manifold model for RTFs is proposed to robustify RTF estimation. Unlike linear methods, this approach provides a high degree of expressiveness by avoiding constraints associated with linearity. The VAE is trained unsupervised using data collected under benign acoustic conditions, enabling it to reconstruct RTFs within the specified enclosure. The method introduces a least squares (LS)-based RTF estimator that is regularized by the trained VAE. This regularization significantly improves the quality of RTF estimates compared to traditional VAE-based denoising methods. In this way, a hybrid model is derived, combining classic RTF estimation with the capabilities of the trained VAE.

In [35], the relation between the graph structure, ML, and GNN is established, emphasizing how the graph structure contributes to the model’s accuracy. Building upon these established foundations, we propose to harness the ML capabilities of GNNs to obtain a more accurate and robust estimator of RTFs in noisy and reverberant environments.

B. Graph Convolution Networks

In this section, we first define the mathematical representation of a graph, then describe the two different types of GCNs, explain the differences between them, and finally, formally define the spatial GCNs.

A graph $\mathcal{G} = (\mathcal{E}, \mathcal{V})$ consists of a set of edges \mathcal{E} and nodes $\mathcal{V} = \{v_1, \dots, v_N\}$, where the edges are assumed to be scalars denoted as $e_{j,i} \in \mathbb{R}$ connecting the j th node to the i th node. Alternatively, the graph can be represented as $\mathcal{G} = (\mathbf{V}, \mathbf{A})$, where $\mathbf{V} \in \mathbb{R}^{N \times d}$ is the nodes’ feature matrix with d the dimension of features and $\mathbf{A} \in \mathbb{R}^{N \times N}$ is the graph adjacency matrix. Denote $\mathcal{N}(i)$ the neighborhood of nodes connected to

node i . The adjacency matrix should then satisfy $\mathbf{A}_{i,j} = 1$ if $j \in \mathcal{N}(i)$ (in the general case, $\mathbf{A}_{i,j}$ can be smaller than 1).

GNNs are a generalization of conventional neural networks designed to process non-Euclidean inputs represented as graphs. Graphs offer considerable flexibility in data representation, and GNNs extend neural network methods to graph-structured data. They achieve this by iteratively propagating information through nodes and edges of the graph, enabling them to capture and exploit the inherent information encoded in the graph structure. A variant of GNN is the GCN, inspired by the principles of learning through shared weights, similar to the approach used in CNNs for image analysis and computer vision. Designing local operations with shared weights is the key to efficient learning on graphs. This involves message passing between each node and its neighbors, facilitated by the shared weights. The use of shared weights, implying parameter sharing across different parts of the graph, enhances the efficiency and scalability of the learning process.

Current GCNs algorithms can be categorized into spectral-based and spatial-based. Spectral GCN relies on the principles of spectral graph theory [36], [37]. This involves processing the graph through the eigendecomposition of the graph Laplacian, which is used to compute the Fourier transform of a graph signal. This, in turn, defines graph filtering operations [18], [38]–[40]. In contrast, spatial-based GCN operates on the principle of message passing. In this approach, each node aggregates information from its local neighborhood. The number of neighbors determines the amount of information aggregated. This aggregation process allows the model to capture local graph structure and node features [21], [22], [35], [41]–[45]. Spatial GCNs can operate locally on each node without considering the entire graph, making them well-suited for node-specific tasks. Given that our problem, as indicated by the graph construction, involves a node-specific task, we will focus on spatial-based GCNs from this point onward. In the sequel, we will elaborate on the spatial GCN.

C. Spatial GCN

Much like the convolutional operation employed by conventional CNNs for image processing, spatial-based methods extend this concept to define graph convolutions based on the spatial relations among nodes. In this analogy, images can be seen as a specific type of graph, where each pixel serves as a node, and direct connections exist between each pixel and its adjacent counterparts. In a CNN, the operation involves computing the weighted average of pixel values for the central node and its neighbors across each channel. In GCNs, the representation of each node is updated by merging its features with those of its neighbors. Borrowing from the CNN terminology, this operation is called *convolution*, or neighborhood aggregation. Unlike traditional convolution in CNNs, which uses scalar multiplications, in GCNs, each node relation — akin to “pixels” in a convolutional kernel — is defined by a small neural network. This neural network can take various forms, such as a nonlinear activation function,

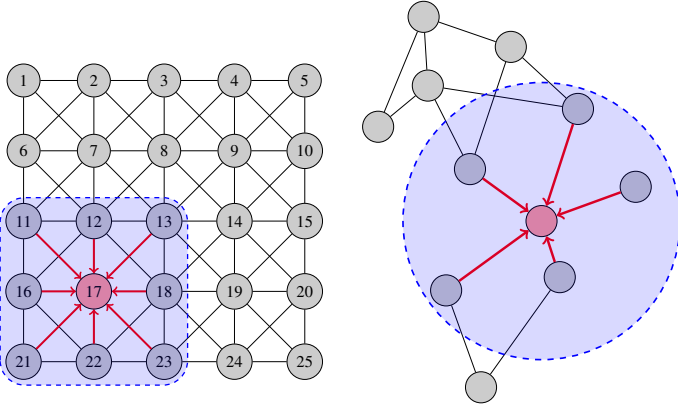


Fig. 1: 2D convolution vs. graph convolution. **Left:** In conventional 2D convolution on an Euclidean input, such as an image, the central pixel (depicted in red) of the next layer is calculated as a weighted average of itself and its neighbors, determined by the kernel size. The input is ordered and numbered accordingly. **Right:** In spatial graph convolution, the representation of the central node in the next layer is computed by aggregating features from neighboring nodes, with no regard to the order of neighbors or fixed graph size. (inspired by [46]).

a linear transformation, an multi-layer perceptron (MLP), or others.

The permutation invariance observed in graph operations significantly differs from classical deep neural networks (DNNs) designed for grid-structured data. This invariance implies independence from the order of neighboring nodes, as there is no canonical way to arrange them. Consequently, a substantial distinction emerges between the kernels of CNNs and those of GCNs. The former leverages the knowledge of the neighbors' ordering by assigning varying weights during convolution. In contrast, GCNs treat the node relationships without assuming any specific order, leading to neural network weights that generalize across all neighbors. These weights are shared across all neighboring nodes and the entire graph. A schematic comparison between 2D convolution and graph convolution is depicted in Fig. 1.

A spatial GCN comprises a sequence of graph convolution layers. The nodes' representations undergo two fundamental steps within each layer: 1) aggregation of features from neighboring nodes and, subsequently, 2) a nonlinear transformation. Each convolutional layer is often implemented as MLPs. The initial representation of nodes at the input to the first convolutional layer relies on their input features.

Before training a GCN, a crucial factor to consider is the network's depth, determining how many neighbor levels are used for information aggregation. As the depth increases, information aggregation expands exponentially [47]. In this

work, we chose not to aggregate information from second-order neighbors (i.e., neighbors of neighbors). The reasons for this decision will be elaborated in Sec. V.

While most existing algorithms primarily focus on tasks like classification, segmentation, and clustering, we aim to extend the capabilities of GCNs to address the more challenging problem, the regression on graph-structured data. Specifically, our goal is to use GCNs to learn representations of graph nodes, where each node is associated with a high-dimensional, continuous-value vector. This approach involves developing a supervised learning algorithm that performs regression directly on these node vectors, considering the graph structure and inter-node relationships. By leveraging GCNs, we seek to capture the intrinsic geometry of the graph and the interactions between nodes, leading to more accurate and meaningful predictions.

IV. RTF-BASED MVDR BEAMFORMERS

This section overviews RTF-based beamforming for speech enhancement using microphone arrays. The MVDR beamformer will be the backbone algorithm throughout the paper. In the noisy case, we utilize the generalized eigenvalue decomposition (GEVD) to estimate the RTFs. We also describe other RTF estimation procedures. The main contribution of the paper, namely the robust RTF estimation, will be detailed in Sec. V.

A. GEVD-Based RTF Estimation - A Concise Overview

In [48], [49], it was demonstrated that the RTF could be estimated through the GEVD of the spatial correlation matrices of the noisy signal segments $\Phi_{rr,\ell}(k)$ ² and of the noise-only signal segments $\Phi_{vv,\ell}(k)$. The latter is estimated from noise-only segments assumed to be available. Here, ℓ represents the source position index. The RTF is determined by solving

$$\Phi_{rr,\ell}(k)\varphi_\ell(k) = \mu_\ell(k)\Phi_{vv,\ell}(k)\varphi_\ell(k). \quad (5)$$

Using $\varphi_\ell(k)$, the generalized eigenvector corresponding to the largest generalized eigenvalue $\mu_\ell(k)$, we can obtain the vector of RTFs using the following normalization:

$$\tilde{\mathbf{h}}_{\text{gevd},\ell}(k) = \frac{\Phi_{vv,\ell}(k)\varphi_\ell(k)}{(\Phi_{vv,\ell}(k)\varphi_\ell(k))_{\text{ref}}}. \quad (6)$$

For each microphone m , we obtain the corresponding time-domain representation of the RTF, which we denote as relative impulse response (ReIR), by applying inverse fast Fourier transform (iFFT) to $\text{vec}_k\{\tilde{\mathbf{h}}_{\text{gevd},\ell}^m(k)\}$, a concatenated vector across all frequency bins k . The ReIR exhibits a distinct pattern characterized by a prominent peak around zero and a rapid decay on both sides. This characteristic allows us to simplify the estimation process by truncating the ReIR around its central region, thereby reducing the number of data points that need to be estimated. This truncation also results in a smoothness of the RTF in the frequency domain. Specifically,

²In the more general form, it can be time-varying, but here we assume that the RTF is time-invariant, and can therefore be estimated by averaging over all active-speech time segments.

we truncate the ReIR to $n = -n_{\text{non-causal}}, \dots, n_{\text{causal}}$ taps. We denote the truncated ReIR as $\bar{h}_{\text{gevd}}^m(n)$, for $m = 1, \dots, M-1$ and $n = -n_{\text{non-causal}}, \dots, n_{\text{causal}}$. We omit the index 0 because it corresponds to the reference microphone, and its ReIR is trivial.

B. The Oracle RTF Estimation

The clean, oracle, RTF estimation procedure is now discussed. In the graph construction described later, the oracle ReIRs will serve as the features of the graph vertices.

We obtain the oracle RTF by applying the GEVD procedure to noiseless training recordings. In the absence of noise, $\Phi_{vv,\ell}(k)$ in (5) is substituted by an identity matrix, simplifying (5) to an eigenvalue decomposition (EVD) problem. After the EVD application, similar to the noisy case, we apply an iFFT followed by a truncation operation to the tap range $n = -n_{\text{non-causal}}, \dots, n_{\text{causal}}$. These clean, truncated ReIRs are denoted as $\bar{\mathbf{h}}_{\text{oracle},\ell}^m$.

C. Nomenclature

This section defines the methods and notations used in this paper. Let ℓ represent a general index of the train and test data. We define:

- $\bar{\mathbf{h}}_{\text{alg},\ell}^m = \text{vec}_n\{\bar{h}_{\text{alg},\ell}^m(n)\}$: Concatenation of all taps $n = -n_{\text{non-causal}}, \dots, n_{\text{causal}}$.
- $\mathbf{h}_{\text{alg},\ell}(k) = \text{vec}_m\{h_{\text{alg},\ell}^m(k)\}$: Concatenation of all microphones for all frequency bins k^3 .

Henceforth, we distinguish between train and test position indices: α for train and β for test.

Define $\bar{h}_{\text{oracle},\alpha}^m(n)$ for $\alpha = 1, \dots, N_{\text{train}}$, $m = 1, \dots, M-1$, and $n = -n_{\text{non-causal}}, \dots, n_{\text{causal}}$ as the ReIR associated with the α -th training location and the m -th microphone. Further, let $\bar{\mathbf{h}}_{\text{oracle},\alpha}^m = \text{vec}_n\{\bar{h}_{\text{oracle},\alpha}^m(n)\}$ be the corresponding vector formed by concatenating all taps. The set of all ReIR training points associated with the m -th microphone is denoted as $\bar{\mathcal{H}}^m = \{\bar{\mathbf{h}}_{\text{oracle},\alpha}^m\}_{\alpha=1}^{N_{\text{train}}}$.

Let $\mathbf{h}_{\text{alg},\beta}(k) = \text{vec}_m\{h_{\text{alg},\beta}^m(k)\}$ be an RTF vector from the test dataset at the β -th test position, where $\beta = 1, \dots, N_{\text{test}}$. Here, $\text{alg} \in \{\text{gevd}, \text{oracle}, \text{gcn}, \text{mp}\}$ represents the algorithm used to obtain the RTF:

- **gevd**: Noisy RTF estimated by the GEVD procedure, followed by iFFT, truncation, and fast Fourier transform (FFT).
- **oracle**: Clean RTF estimated in noiseless environments, followed by iFFT, truncation, and FFT.
- **gcn**: RTF obtained by applying the GCN (our method).
- **mp**: The manifold projection (MP)-based competing method [25], explained in Sec. VI.

D. The MVDR Beamformer

Let $\mathbf{h}_{\text{alg},\beta}(k)$ represent RTFs from our test data at a specific position that is estimated by one of the designated algorithms. Define $\Phi_{vv,\beta}(k)$ as the $M \times M$ spatial power spectral density

³We include the reference microphone RTF (equal to 1) in the concatenated vector to obtain the full M -dimensional vector.

(PSD) matrix at the k -th frequency bin of the noise signals. It is assumed that noise-only segments are available and can be identified, e.g., by applying a voice activity detection (VAD).

The MVDR beamformer is a spatial filter designed to minimize the noise power at its output while maintaining a distortionless response toward the desired source. Its optimal weights are given by:

$$\mathbf{w}_{\text{alg},\beta}^{\text{MVDR}}(k) = \frac{\Phi_{vv,\beta}^{-1}(k)\mathbf{h}_{\text{alg},\beta}(k)}{\mathbf{h}_{\text{alg},\beta}(k)\mathbf{H}\Phi_{vv,\beta}^{-1}(k)\mathbf{h}_{\text{alg},\beta}(k)}. \quad (7)$$

Here, we follow [1] and subsequent publications and use the RTF as the steering vector of the MVDR beamformer. It was shown in multiple works (see, e.g., [16], [17]) that implementing an MVDR beamformer with the RTF rather than with a steering vector solely based on the DOA of the desired source, yields significantly improved results in reverberant environments.

E. Block Diagram of the Proposed System

Figure 2 summarizes the proposed framework for robust microphone array speech enhancement. The framework comprises several blocks. First, the ReIRs, denoted as $\bar{\mathbf{h}}_{\text{gevd}}^m$, are estimated from the noisy input signals. The feature extraction follows GEVD, iFFT, and truncation. Next, the ReIR estimates are updated using oracle ReIRs that were estimated in the same acoustic environment, yielding a more robust estimate of the ReIR, denoted as $\bar{\mathbf{h}}_{\text{gcn}}^m$. Finally, these updated ReIRs are transformed to the frequency domain using FFT, followed by a concatenation of all microphones to form the RTF vector. The enhanced RTF vector is then used to construct the MVDR beamformer that is applied to the noisy input signals to obtain an estimate of the desired source signal. In the next section, we describe the proposed GCN-based, robust RTF estimation.

V. PEERRTF: A GCN-BASED ROBUST RTF ESTIMATION

This section introduces the proposed robust RTF estimation method. We delve into the preprocessing of the data, the construction of a feature vector, and the associated graph data. Finally, we explore the derived GCN architecture and our objective functions. Our method is inspired by the manifold-learning approaches presented in [24], [25]. In the current contribution, we propose to harness a modern ML methodology based on DNN. Similar to the previous works, our approach leverages prior knowledge regarding the acoustic environment to project the noisy samples onto the manifold. Given that our data is represented as a graph, we utilize message-passing techniques to achieve this goal.

A. Graph Representation of ReIRs

The learning process involves understanding the relations between neighboring entities. In our case, this requires learning the GNN weights. Before training, we need to construct the graph, including defining the relations between nodes.

This section describes the feature vectors, the graph construction, and the training procedure.

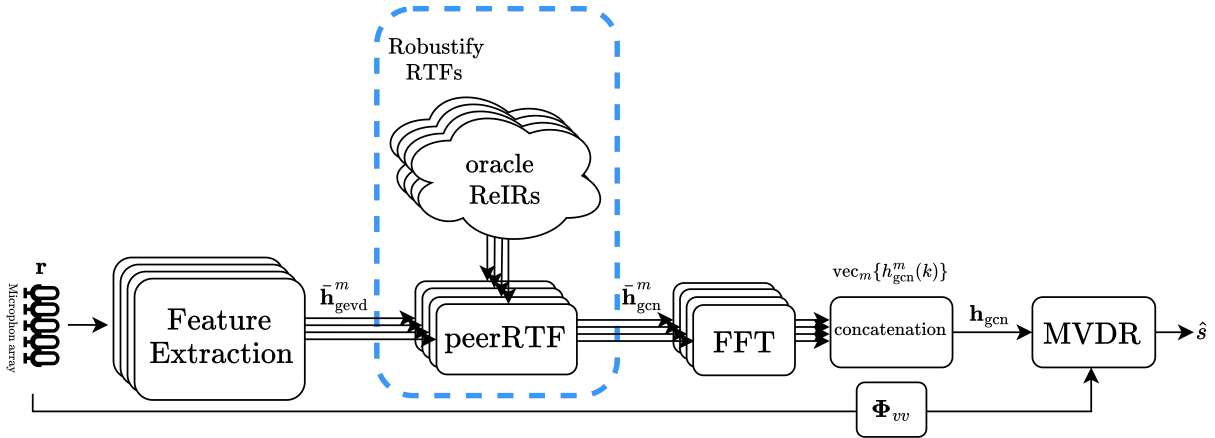


Fig. 2: A general block diagram of robust RTF-based beamforming. First, the noisy signal is used to estimate the ReIR using GEVD, iFFT, and truncation, resulting in initial ReIRs, denoted as $\bar{\mathbf{h}}_{\text{gevd}}^m$. These initial ReIRs are then enhanced using the GCN architecture and oracle ReIRs from the same acoustic environment, resulting in robust ReIRs, denoted as $\bar{\mathbf{h}}_{\text{gcn}}^m$. The robust ReIRs are then transformed to the frequency domain using FFT, followed by concatenation across the microphone index. Finally, using the enhanced RTF, the MVDR beamformer is applied to estimate the enhanced recording.

1) *Feature Vector*: RTFs-based beamformers are applied in the frequency domain. However, as we already mentioned, the corresponding time-domain representation features a peak around tap zero and rapid decay on both sides. This characteristic allows us to simplify the estimation by truncating the ReIR around the central region, reducing the number of data points, and smoothing the RTF in the frequency domain. A typical ReIR associated with AIRs from the MIRaGe dataset [50], with reverberation time of $T_{60} = 300\text{ms}$, is depicted in Fig. 3. This example represents a typical ReIR associated with one of the grid points. The RTF vector is obtained using the GEVD procedure in (6) in noiseless conditions, i.e., the identity matrix substitutes the spatial correlation matrix of the noise. The clean microphone signals are obtained by convolving AIRs from the MIRaGe dataset with pink noise input signal. We chose one of the $M - 1$ RTFs obtained from this grid point, transformed it to the time-domain and finally truncated it to obtain the ReIR.

Applying the GCN to the time-domain representation rather than the frequency-domain representation circumvents the need to work with complex-valued neural networks. When dealing with an array of M microphones, $M - 1$ RTFs are attributed to each speaker location, as the RTF between the reference microphone and itself is trivial. These $M - 1$ components are usually estimated independently. Truncating the ReIR reduces the feature dimension, thereby enhancing learning abilities compared to using the full ReIR. The resulting feature dimension is $d = n_{\text{non-causal}} + n_{\text{causal}}$. We will independently apply our method to each microphone pair and construct $M - 1$ graphs. Through this construction, each room location is attributed with $M - 1$ features, each of which has a dimension of d .

2) *Graph Construction*: We now turn to the graph construction stage. We have a separate graph for each microphone pair comprising N_{train} nodes. The set of N_{train} node

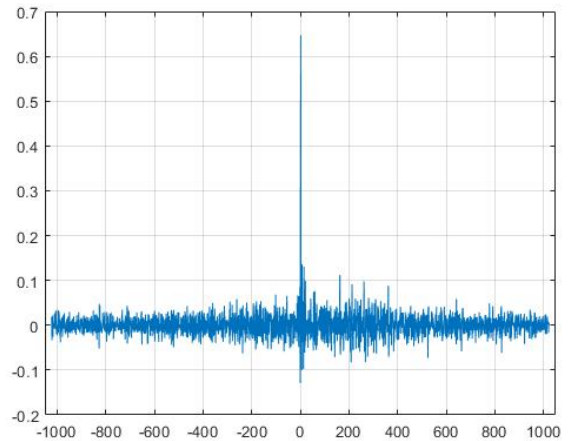


Fig. 3: Typical ReIR corresponding to room impulse responses (RIRs) from the the MIRaGe database with a reverberation time of $T_{60} = 300\text{ms}$.

features are the ideal ReIRs that were estimated in noiseless environment, $\bar{\mathbf{h}}_{\text{oracle},\alpha}^m$. We denote the set of features as $\bar{\mathcal{H}}^m$, $m = 1, \dots, M - 1$.

The graph is constructed by applying a \mathcal{K} nearest neighbors (\mathcal{KNN}) procedure. We decided to utilize the \mathcal{KNN} procedure since it selects the most similar ReIRs (in terms of Euclidean distance) from the dataset, allowing us to effectively robustify the ReIRs for the noisy feature vectors, by leveraging information from relevant neighbors. As mentioned, we construct a separate graph for each microphone pair. This helps to capture specific relationships and dependencies within the data.

3) *Training Procedure*: In the training stage, our goal is to learn optimal weights that will enable noisy feature

enhancement during testing. We begin with \bar{H}^m . For each training step, we select one training position and perform the following steps: 1) exclude the clean feature vector associated with this selected position, $\bar{h}_{\text{oracle},\alpha}^m$ from all $M - 1$ graphs; 2) incorporate noisy feature vectors, $\bar{h}_{\text{gevd},\alpha}^m$, related to this same position into the graphs using the \mathcal{K} NN procedure.

Consequently, each training example comprises $N_{\text{train}} - 1$ clean feature vectors and one noisy feature vector from the same position that was removed.

4) *Test Procedure*: In the test phase, we have N_{test} vanilla ReIRs that are estimated in a noisy scenario: $\bar{h}_{\text{gevd},\beta}^m$ where $\beta = 1, \dots, N_{\text{test}}$. We process these test samples sequentially, adding one test example to the existing trained graphs at each step. Each test sample represents a set of noisy feature vectors, with each vector corresponding to an ReIR for a specific microphone pair. For each ReIR (corresponding to one microphone pair), the new node (test sample) is connected to the existing graph structure using the \mathcal{K} NN procedure. After adding the test sample, the graph now comprises $N_{\text{train}} + 1$ nodes, with a feature vector of dimension d associated with each node. This process is repeated for all $M - 1$ graphs corresponding to the $M - 1$ microphone pairs. Consequently, at each step, we add one new node to each of the $M - 1$ graphs.

B. The GCN Architecture

A key factor in the success of CNNs is their ability to design and reliably train deep models that extract higher-level features at each layer. This process is facilitated by weight sharing, where the same kernel is applied across each channel.

In contrast, training deep GCN architectures is not as straightforward, and several works have studied their limitations [23], [46], [51], [52]. Stacking more layers into a GCN leads to the typical vanishing gradient and over-smoothing problems. Due to these limitations, most state-of-the-art GCNs are not deeper than four layers [23]. In each layer, the transformation function is usually a single, shallow, fully-connected (FC) layer followed by a non-linearity. Such shallow architectures are sufficient for classification, segmentation, clustering, and recommendation tasks. However, these shallow networks lack the expressive power to perform more challenging tasks, such as regression on high-dimensional data. In our scenario, where nodes represent truncated ReIR associated with different room positions, we choose not to aggregate information from second-order neighbors. However, we implement a deep network with three layers, ensuring sufficient expressive power for regression tasks on a high-dimensional abstract manifold. Drawing inspiration from [22], which learns 3D manifolds from point clouds, we structured our architecture accordingly. Drawing an analogy to convolution in images, we consider $\bar{h}_{\text{gevd},i}^m$ as the central pixel and $\bar{h}_{\text{oracle},i_j}^m, j \in \mathcal{N}(i)$ as a patch around it. To calculate the contribution of each neighbor $\bar{h}_{\text{oracle},i_j}^m$ within each graph, we concatenate the feature vector of the central node $\bar{h}_{\text{gevd},i}^m$ with the feature vector of the neighbor $\bar{h}_{\text{oracle},i_j}^m$ and pass this concatenated vector through the neural network. The neural

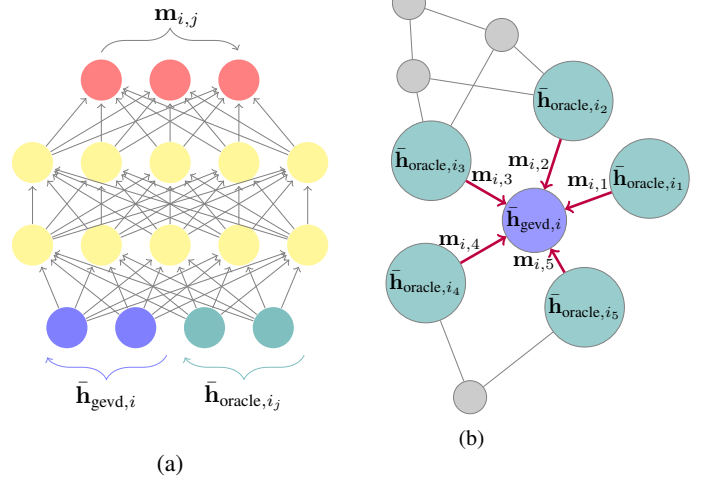


Fig. 4: Left: The message $m_{i,j}$ passed from the j th neighbor of the i th node is calculated by concatenating $\bar{h}_{\text{gevd},i}$ and $\bar{h}_{\text{oracle},i_j}$ and passing this concatenation through the neural network.

Right: The representation of the i th node at the output is calculated by aggregating the messages from all the nodes in $\mathcal{N}(i)$. For each microphone, there is a separate graph and the neighbors are arbitrarily numbered.

*inspired by [22]

network output is then aggregated from all neighbors of $\bar{h}_{\text{gevd},i}^m$ $\mathcal{N}(i)$. When deliberating on selecting an aggregation function, it is essential to consider the essence of our regression task on the manifold. Given that our objective is to predict a continuous value falling within the range of the input values, this criterion guides our choice of aggregation functions. In this context, sum and max are not optimal choices. Instead, we opt for the mean operation as $\frac{1}{|\mathcal{N}(i)|} \sum_{j \in \mathcal{N}(i)}$. Figure 4 details the selected architecture.

We utilized message passing, one of several commonly used methods in GNN. As mentioned, this process involves information exchange between nodes and their neighbors on the graph, enabling them to update their knowledge based on local interactions. Message passing facilitates effective learning and inference in graph-based models. For our graphs, we have \mathcal{K} representing the number of neighbors.

Our neural network architecture consists of three FC layers, followed by an activation function. The input to the network is a concatenated vector of length $2d$, and the architecture can be represented as follows: $2d \rightarrow 2d \rightarrow 2d \Rightarrow d$. Here, each \rightarrow represents a single FC layer followed by a rectified linear unit (ReLU) activation function, while \Rightarrow denotes only a FC layer.

Our GCN architecture employs two levels of weight sharing. The first level, a standard convention in GCNs, involves sharing weights across all node connections within each graph. This allows the network to process nodes uniformly regardless

of their position in the graph. The second level, specific to our approach, extends weight sharing across all $M - 1$ graphs corresponding to different microphone pairs. This means that a single set of GCN parameters is used to simultaneously process all microphone pair graphs. To evaluate the effectiveness of this approach, we experimented with an alternative configuration. In this alternative, we used $M - 1$ individual GCNs, each dedicated to a specific microphone pair graph, working independently without sharing weights across different graphs. This setup allowed for specialized processing of each microphone pair’s data, resulting in a simpler training procedure with more parameters. However, our experiments showed that this separate GCNs architecture did not yield any significant performance improvements over the shared-weight approach. Given these results, we opted for the shared-weight architecture across all graphs. This decision offers two key advantages: 1) it significantly reduces the overall model complexity by decreasing the number of parameters, and 2) it provides flexibility, allowing the architecture to adapt easily to varying numbers of microphone pairs, a significant consideration in practical applications. Algorithm 1 succinctly summarizes the procedural steps for GCN-based RTF estimation. Figure 5 describes the full architecture.

Algorithm 1: Robust RTF Estimation Using GCN.

Training Stage:

- 1) Given \mathcal{H}^m clean ReIRs build the graphs using \mathcal{KNN} for each microphone pair.
- 2) Select one grid position and remove the clean feature vectors $\bar{h}_{\text{oracle},\alpha}^m$ associated with this location, replace them with noisy feature vectors $\bar{h}_{\text{gevd},\alpha}^m$, and connect them to the graphs using \mathcal{KNN} .
- 3) Train GCN for robust representation of noisy ReIRs. Repeat for the entire dataset until convergence.

Inference Stage:

- 1) For each test sample, add the noisy feature vector $\bar{h}_{\text{gevd},\beta}^m$ to each of the $M - 1$ trained graphs constructed with clean features \bar{H}^m by applying the \mathcal{KNN} procedure.
 - 2) Feed the noisy feature $\bar{h}_{\text{gevd},\beta}^m$ to the trained GCN to improve the estimation of noisy ReIRs nodes. Repeat for all test positions.
-

C. Objective Functions

To efficiently train the model, we examined two alternative objective functions. In the first alternative, we directly optimized the outcome of the GCN, namely the ReIR estimate. In the second alternative, we optimize the output of the MVDR beamformer by adjusting the RTF estimate. The two training objectives are schematically depicted in Fig. 6 and detailed in the sequel.

1) *Direct Optimization of the ReIR:* Inspired from [53], define the signal blocking factor (SBF) as:

$$\text{SBF} = \frac{1}{M - 1} \sum_{m=0, m \neq \text{ref}}^{M-1} 10 \log_{10} \left(\frac{\sum_t x_m^2(t)}{\sum_t d_m^2(t)} \right) \quad (8)$$

where

$$x_m(t) = \{\bar{h}_{\text{oracle}}^m * \tilde{s}\}(t)$$

and

$$d_m(t) = \{\bar{h}_{\text{oracle}}^m * \tilde{s}\}(t) - \{\bar{h}_{\text{gen}}^m * \tilde{s}\}(t).$$

Here, $\tilde{s}(t)$ is the reference signal, $\bar{h}_{\text{oracle}}^m(t)$ is the oracle ReIR corresponding to the m th microphone, and $\bar{h}_{\text{gen}}^m(t)$ is the robust ReIR of the m th microphone. The term $d_m(t)$ is defined as the difference between convolution of $\bar{h}_{\text{oracle}}^m(t)$ and $\tilde{s}(t)$ with the convolution of $\bar{h}_{\text{gen}}^m(t)$ and $\tilde{s}(t)$. This function encourages the robust ReIR to be as close as possible to the oracle ReIR.

2) *RTF Estimation via Beamformer Output Optimization:*

Here we optimize the scale-invariant source-to-distortion ratio (SI-SDR) at the output of the beamformer. The SI-SDR is defined as:

$$\text{SI-SDR}(\tilde{\mathbf{s}}, \hat{\mathbf{s}}) = 10 \log_{10} \left(\frac{\| \frac{\langle \tilde{\mathbf{s}}, \hat{\mathbf{s}} \rangle}{\langle \tilde{\mathbf{s}}, \tilde{\mathbf{s}} \rangle} \tilde{\mathbf{s}} \|^2}{\| \frac{\langle \tilde{\mathbf{s}}, \hat{\mathbf{s}} \rangle}{\langle \tilde{\mathbf{s}}, \tilde{\mathbf{s}} \rangle} \tilde{\mathbf{s}} - \hat{\mathbf{s}} \|^2} \right) \quad (9)$$

where $\tilde{\mathbf{s}}$ represents a concatenation of all samples of the reference source, and $\hat{\mathbf{s}}$ represents the respective vector of all beamformer’s output samples. The SI-SDR loss is a metric commonly used to evaluate the quality of source separation or speech enhancement algorithms [54]. It measures the enhancement quality between the estimated source signal and the true source signal, considering both the distortion and the interference introduced during the enhancement process. This loss term aims to bring the beamformer output closer to the clean reference signal. The RTF estimate should be adjusted accordingly. Additionally, we explore an alternative approach by examining the SI-SDR compared to the output of the oracle RTF beamformer. Here, we compute the MVDR weights using the RTFs estimated under ideal conditions, namely the oracle scenario, and evaluate the resulting SI-SDR compared with this signal. This approach aligns more closely with a supervised paradigm, akin to the RTF level loss. Importantly, it eliminates the necessity for a clean reference signal in the loss function, addressing a common limitation in scenarios where such a reference signal is unavailable. Still, in this objective, we need the oracle RTFs to be available, which is another limitation. We will designate the first version as SI-SDR I and the second as SI-SDR II.

We also incorporate an implementation of short-time objective intelligibility (STOI) as a loss function⁴. This implementation is integrated with VAD for focusing only on the active speech segments. STOI serves as a metric for evaluating the intelligibility of speech signals.

⁴adopted from https://github.com/mpariente/pytorch_stoi.

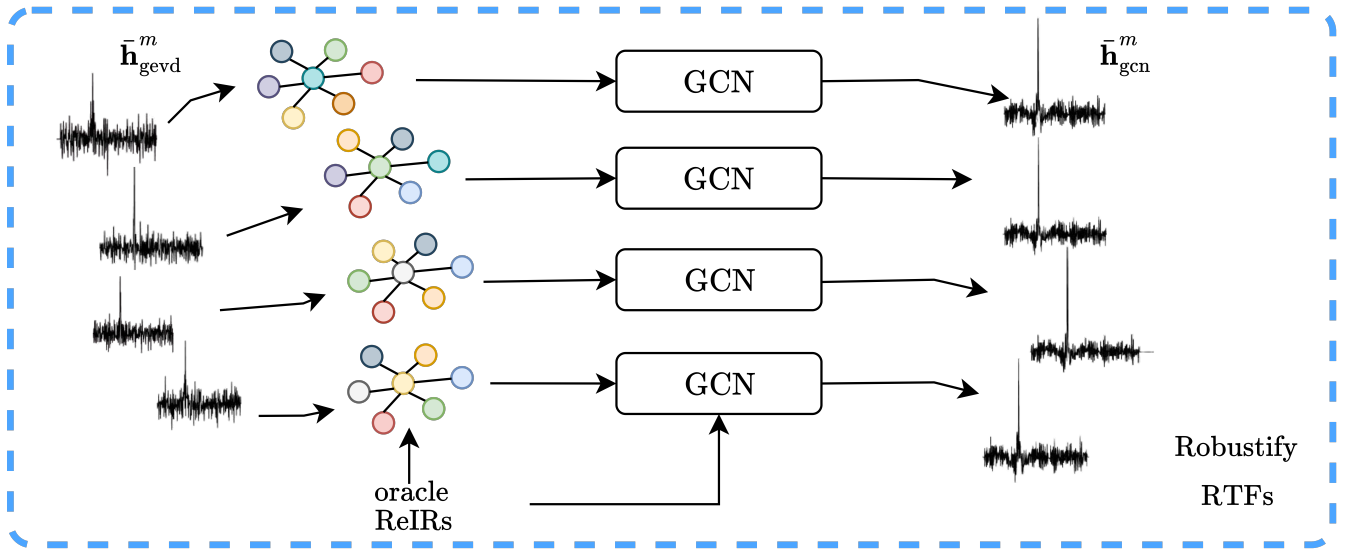


Fig. 5: The robust RTF estimator. The inputs to the system are clean and noisy ReIRs. The clean ReIRs are obtained in the training set, while the noisy ReIRs are estimated at the test phase. The graph is constructed by applying the \mathcal{K} NN procedure. Subsequently, a GCN is applied on the graph, resulting in the robustified ReIRs. Note that there are $M - 1$ independent graphs.

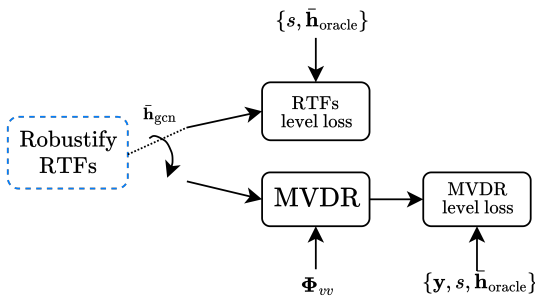


Fig. 6: Two alternative training objectives.

VI. EXPERIMENTAL SETUP AND RESULTS

The proposed method is evaluated using the MIRaGe dataset [50], comprising measured multichannel signals recorded at the Bar-Ilan University acoustic lab. We evaluate the proposed GCN method using various objective and subjective performance measures. Additionally, we explore the impact of the graph structure on the results and compare several objective functions.

A. Experimental Setup:

The database was generated by placing a loudspeaker on a grid of points in a cube-shaped volume with dimensions $46 \times 36 \times 32$ cm. The loudspeaker positions were set every 2 cm along the x and y axes and every 4 cm along the z-axis, totaling $24 \times 19 \times 9 = 4104$ possible source positions (grid vertices). In addition, 16 other positions, referred to as out of grid (OOG), were designated as possible locations for noise sources. A chirp signal was played for each position

in the grid and OOG positions. The setup was recorded using six static linear microphone arrays, each consisting of $M = 5$ microphones with an inter-microphone spacing of $-13, -5, 0, +5, +13$ relative to the central microphone (the reference microphone). Recordings were made at three different reverberation levels: 100, 300, 600 ms.

For our experiments, we utilized microphone array #2, positioned directly in front of the cube at a distance of 2 m from its center. The recordings were randomly split into $N_{\text{train}} = 3500$ training positions, $N_{\text{validation}} = 100$, and $N_{\text{test}} = 504$. We use 2048 frequency bins. After the inverse Fourier transform, we truncate the length of the ReIR to $l_{\text{non-causal}} = 128$ and $l_{\text{causal}} = 256$.

The estimation of the RTFs involves the following steps: 1) using the recorded chirp signals from the MIRaGe database, the AIRs from the source position to the microphone arrays are estimated using a LS procedure; 2) for generating the clean RTFs for the graph construction, pink noise signals covering all relevant frequencies were convolved with the AIRs to generate the desired signal; for generating the noisy signals, we convolved a speech signal with the AIRs and then added pink noise from an OOG location; finally, 3) the RTFs of the noisy utterances were estimated using the procedure in (6), and for the clean RTFs, we used the EVD procedure.

To construct a sufficiently large training set, we add to each of the 3500 clean training speech signals three different noise signals with random SNR from a range of $\text{SNR} \in [-10, 10]$ dB, from 16 different OOG locations, resulting in $3500 \times 3 = 10500$. We set $\mathcal{K} = 5$ as the \mathcal{K} NN parameter.

The network was trained using a linear scheduler with a warmup ratio 0.1, a learning rate of 1×10^{-4} . We chose the

SI-SDR in its second version as the objective function for all reverberation times, incorporating a dropout rate of 0.5 during the training stage over 100 epochs. Our choice of SI-SDR II as the objective function was not arbitrary. After extensive experimentation with various alternatives, we found it to be the most effective for our purposes. The next section provides a detailed comparison of the objective functions we considered, highlighting the advantages that led us to select SI-SDR II for this study. The various parameters are listed in Table I.

TABLE I: Parameters.

Parameter	Description	Value
M	Number of microphones	5
K	Number of frequency bins	2048
$n_{\text{non-causal}}$	Number of taps left of the peak	128
n_{causal}	Number of taps right of the peak	256
\mathcal{K}	Number of neighbors in the graph	5

B. Quality Measure:

The results are analyzed using several quality metrics. The first is the SNR at the beamformer’s output, calculated as:

$$\text{SNR}(\hat{\mathbf{s}}, \hat{\mathbf{v}}) = 10 \log_{10} \left(\frac{\|\hat{\mathbf{s}}\|^2}{\|\hat{\mathbf{v}}\|^2} \right). \quad (10)$$

Here, $\hat{\mathbf{s}}$ represents the speech component at the beamformer output, with all samples concatenated into a vector, and $\hat{\mathbf{v}}$ represents the corresponding noise component at the beamformer output. As our dataset is simulated, we can access the noise and the signal separately. Then, using the linearity of the MVDR beamformer, $\hat{\mathbf{s}}$ and $\hat{\mathbf{v}}$ can be easily obtained.

The quality of the output signal was also assessed using STOI [55] (for the intelligibility) and deep noise suppression mean opinion score (DNSMOS) [56] (for speech quality). We also examined the SI-SDR (9) in its first variant, comparing the beamformer’s output to the reference signal.

C. Baseline Methods:

The proposed GCN-based method is compared with three other baselines, employing the MVDR beamformer. Two basic baselines are RTF-based MVDR beamformers. The first is the traditional GEVD procedure for RTF estimation, using the truncated ReIR. The second method uses the oracle RTF estimated under noise-free conditions. We also truncate the corresponding ReIR in this case for fair comparison.

The third is utilizing the method introduced in [25] to robustify the RTF estimation. This method is dubbed MP learning. For MP, two parameters need to be set: ϵ , the kernel scale parameter, and λ , the number of dominant eigenvalues in the algorithm. Specifically, we chose $\epsilon = 0.3$ for all reverberation times, and λ varied depending on the reverberation level. For $T_{60} = 100$ ms, we selected $\lambda = 12$, for $T_{60} = 300$ ms, $\lambda = 5$, and for $T_{60} = 600$ ms, $\lambda = 15$. Similar to the previous methods, we also applied truncation to the ReIR to guarantee fair comparison across all methods.

D. Results:

Figures. 7,8,9 depict the SNR_{out} , STOI, and DNSMOS measures as a function of the input SNR, for $T_{60} = 100, 300, 600$ ms, respectively, comparing the proposed method (peerRTF) with GEVD, Oracle, and the MP algorithm.

As can be seen, the proposed method outperforms the vanilla GEVD-based beamformer in terms of speech intelligibility across all SNR and reverberation levels. Compared to the MP beamformer, there is an improvement in almost all SNR levels and reverberation time. The SNR at the beamformer output is consistently higher than that of the vanilla GEVD and MP beamformers across all input SNR levels and reverberation conditions. Furthermore, our method even outperforms the oracle RTF in several SNR levels and reverberation times.

These advantages are also subjectively demonstrated in Fig. 10 by sonogram assessment for a randomly chosen example from the test set at $\text{SNR}_{\text{in}} = -10$ dB and $T_{60} = 600$ ms. We compare the reference signal (the target), the noisy signal, and RTF-based MVDR beamformer and the proposed peerRTF beamformer. We also provide a zoom-in sub-figure to assess the fine details. When comparing the output of the beamformer to the reference signal, it is evident that the peerRTF output is more close to the reference signal than the GEVD output. For instance, in the upper rectangle, we can observe a strong frequency bin at the GEVD output, which does not appear in either the reference signal or the peerRTF output. In the lower rectangle, there is a small speech gap that is present in both the reference signal and the peerRTF output but missing in the GEVD output. Additionally, the peerRTF sonogram exhibits less noise compared to the GEVD output. This suggests that the peerRTF output has fewer artifacts and less noise than the GEVD output. Sound samples are available on our project page.⁵

E. Alternative Loss Functions and Graph Structure

In this section, we will compare different graph structures to demonstrate how the neighboring nodes affect performance. Specifically, we aim to highlight that considering the neighbors of each node in the graph can lead to improved results, as opposed to enhancing each node in isolation without taking information from the neighbors into account. Additionally, we will evaluate various objective functions and assess different methods to robustify the RTFs.

Our evaluation focuses on challenging acoustic conditions, specifically for a reverberation time of $T_{60} = 600$ ms and a SNR of -10 dB. These conditions are particularly unfavorable for the vanilla GEVD-based estimator, thus providing a significant challenge test for our proposed improvements.

First, we will compare different graph structures to assess the impact on the robustness of RTFs. Specifically, we will examine two scenarios: single nodes without neighbors (graphs without edges) versus nodes influenced by their neighbors. This comparison is driven by a provocative hypothesis suggesting that feature enhancement is primarily due to the network’s

⁵Project Page: <https://peerrtf.github.io/>

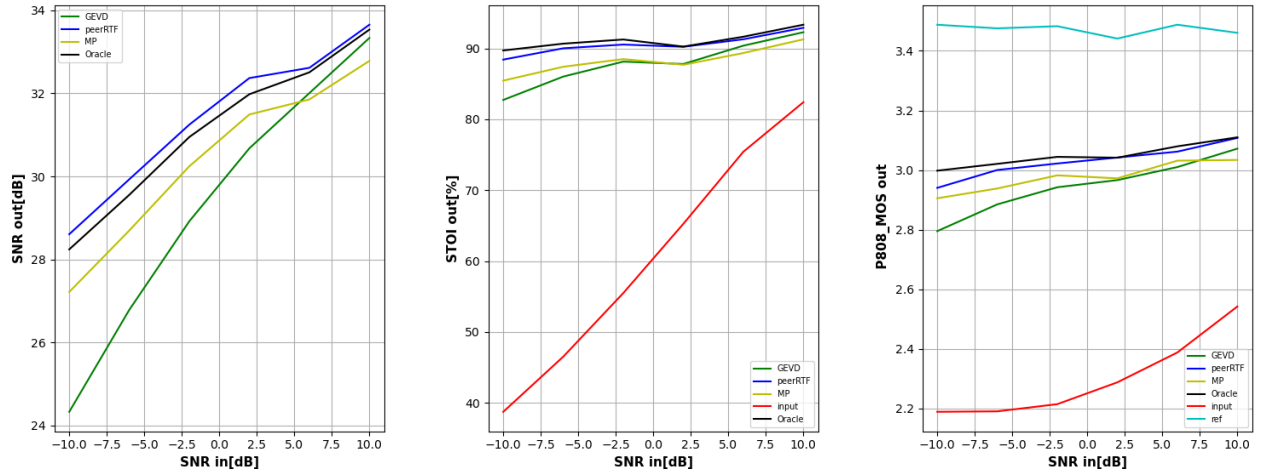


Fig. 7: SNR_{out}[dB] (left), STOI[%] (middle) and DNSMOS(right) for $T_{60} = 100$ [ms].

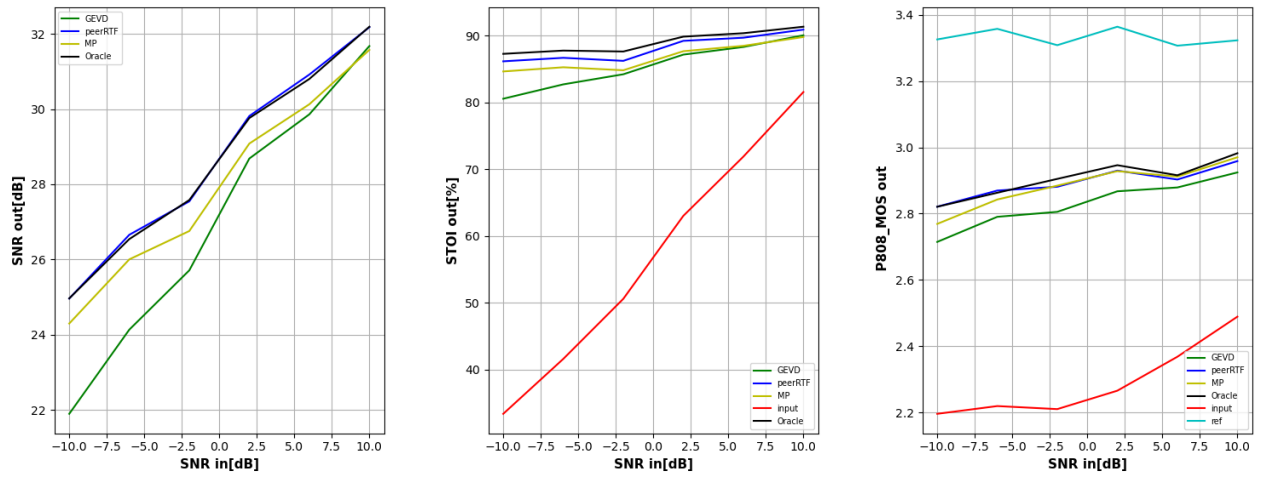


Fig. 8: SNR_{out}[dB] (left), STOI[%] (middle) and DNSMOS(right) for $T_{60} = 300$ [ms].

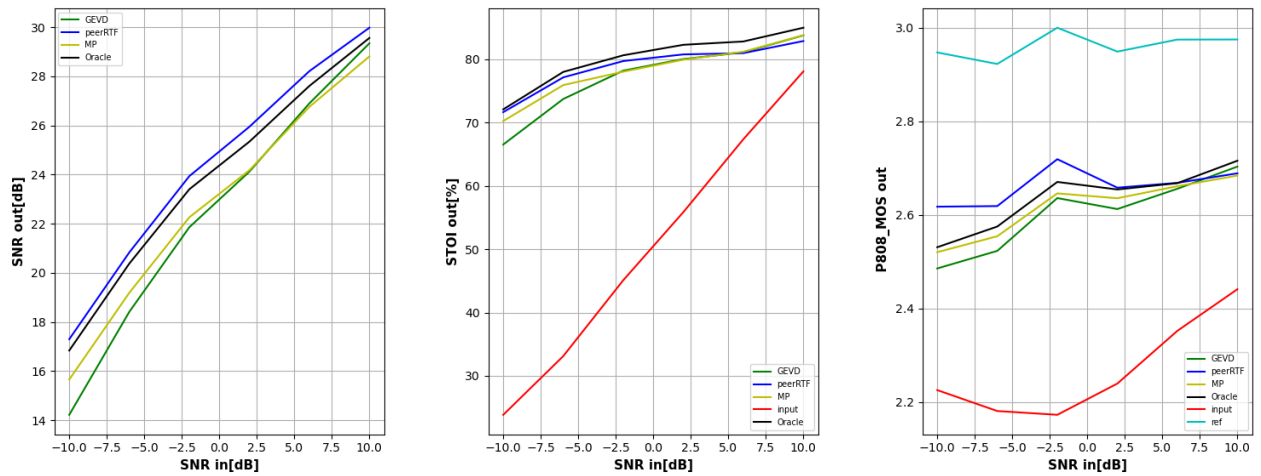


Fig. 9: SNR_{out}[dB] (left), STOI [%] (middle) and DNSMOS(right) for $T_{60} = 600$ [ms].

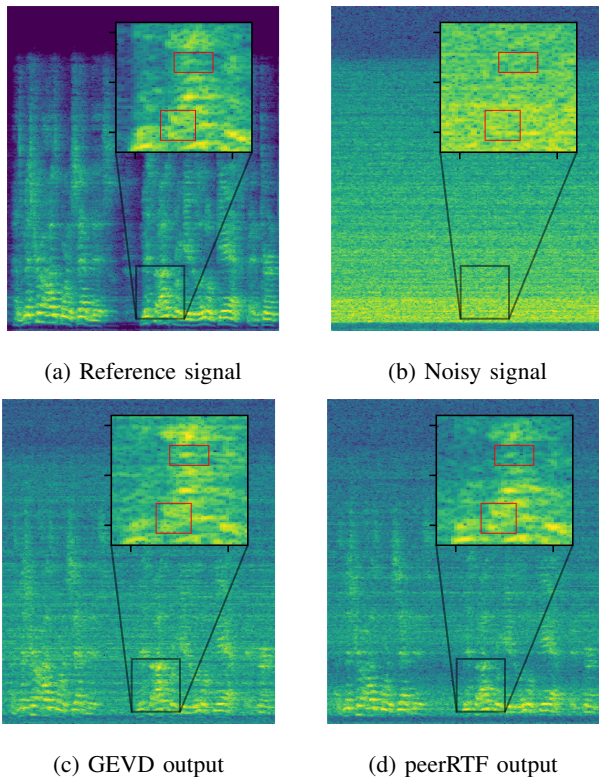


Fig. 10: Sonograms: $\text{SNR}_{\text{in}} = -10$ dB and $T_{60} = 600$ ms.

power rather than the information passed from other nodes. We aim to determine whether neighbors genuinely influence individual nodes and the graph as a whole or if the network’s inherent strength makes such connections superfluous.

In Table II, we compare our method to the self-RTF, which is the disconnected graph. This comparison allows us to evaluate the importance of graph connectivity in our approach versus a structure where nodes operate independently without neighbor influences. Additionally, we include all the methods we discussed earlier in this comparison. In the self-RTF architecture, neighboring clean RTFs are not utilized; instead, the input to the regression network is solely using the noisy RTF. To ensure a fair comparison, all other factors were trained similarly to the peerRTF scheme. Results demonstrate that our method consistently outperforms the self-RTF structure across all quality measures. Interestingly, for several distortion measures, specifically SI-SDR, DNSMOS, and SNR—we observed that even the input for the network (GEVD, representing the noisy RTF) outperformed the self-RTF scenario. This finding is particularly significant as it highlights two key points: (1) the crucial role played by incorporating neighbor information in the network’s processing and (2) the limitations of processing isolated nodes. Our network’s superior performance emphasizes the importance of leveraging the information from the neighbors.

Next, we examine the impact of different objective functions. In Table III, we train and evaluate the GCN with different objective functions. It is evident that each quality

TABLE II: The importance of node neighbors.

Model	STOI	ESTOI	SISDR	P808 MOS	SNR
Unprocessed	23.85	9.32	-10.2	2.22	-10
Reference	-	-	-	2.94	-
Oracle	72.07	55.95	0.57	2.53	16.83
GEVD	66.52	49.5	-3.33	2.52	14.21
MP	70.23	54.21	-1.77	2.52	15.65
peerRTF	71.63	55.53	0.46	2.62	17.3
Self-RTFs	68.06	51.54	-6.2	2.48	12.29

measure benefits differently from the objective function. For instance, using the STOI objective for training highlights the STOI and extended short-time objective intelligibility (ESTOI) measures, as expected. Similarly, SI-SDR I function emphasizes both SI-SDR and SNR, reflecting their focus on SNR and signal distortion. In contrast, the SI-SDR II loss, which we discussed earlier, utilizes the oracle RTF and provides more direct supervision compared to the other objectives that rely on the clean speech signal. This approach mainly improves the DNSMOS metric. Given these varied outcomes, we selected the objective function that provides a balanced improvement across all metrics as our preferred choice.

TABLE III: Objectives measures.

Model	STOI	ESTOI	SISDR	P808 MOS	SNR
Unprocessed	23.85	9.32	-10.2	2.22	-10
Reference	-	-	-	2.94	-
Oracle	72.07	55.95	0.57	2.53	16.83
GEVD	66.52	49.5	-3.33	2.52	14.21
MP	70.23	54.21	-1.77	2.52	15.65
SI-SDR I	72.52	57.21	2.34	2.57	17.96
SI-SDR II	71.63	55.53	0.46	2.62	17.3
SBF	71.32	55.53	-0.5	2.52	15.5
STOI	72.87	57.32	-2.23	2.51	15.12

VII. CONCLUSION

In this paper, we have presented a novel RTF identification method that relies on learning the RTF manifold using a GCN to infer a robust estimation of the RTF in a noisy and reverberant environment. This approach represents a significant advancement in acoustic beamforming, specifically through the application of GCNs to this domain. To the best of our knowledge, this is the first time GCNs have been employed for robust RTF estimation, offering a unique way to capture and leverage the complex spatial relationships within the RTF manifold. By utilizing GCNs, our method explores a different approach to learning-based acoustic processing. It aims to account for the interconnected nature of spatial acoustic information, potentially offering improved robustness in RTF estimation under challenging acoustic conditions. The results presented here confirm the robustness of this method, demonstrating the advantages of directly applying a learning algorithm to the graph that represents the manifold. This approach is superior to learning a projection of the graph into

Euclidean space, which involves flattening the manifold and performing operations within that space.

There are still several opportunities to enhance the GCN model and its robustness. Future work could focus on strengthening the model architecture for better performance and refining the graph structure. For instance, exploring more sophisticated methods for selecting neighbors and defining edges could be beneficial. Additionally, we have yet to evaluate the model with multiple sources, where the accuracy of RTFs would be even more critical.

REFERENCES

- [1] S. Gannot, D. Burshtein, and E. Weinstein, "Signal enhancement using beamforming and nonstationarity with applications to speech," *IEEE Tran. on Signal Proc.*, vol. 49, no. 8, pp. 1614–1626, 2001.
- [2] S. Markovich-Golan and S. Gannot, "Performance analysis of the covariance subtraction method for relative transfer function estimation and comparison to the covariance whitening method," in *IEEE Inter. Conf. on Acoustics, Speech and Signal Proc. (ICASSP)*, 2015, pp. 544–548.
- [3] X. Li, L. Girin, R. Horaud, and S. Gannot, "Estimation of relative transfer function in the presence of stationary noise based on segmental power spectral density matrix subtraction," in *IEEE Inter. Conf. on Acoustics, Speech and Signal Proc. (ICASSP)*, 2015, pp. 320–324.
- [4] O. Shalvi and E. Weinstein, "System identification using nonstationary signals," *IEEE Transaction on Signal Proc.*, vol. 44, no. 8, pp. 2055–2063, 1996.
- [5] Z. Koldovský, J. Málek, and S. Gannot, "Spatial source subtraction based on incomplete measurements of relative transfer function," *IEEE/ACM Tran. on Audio, Speech, and Language Proc.*, vol. 23, no. 8, pp. 1335–1347, 2015.
- [6] Y. R. Zheng, R. A. Goubran, and M. El-Tanany, "Robust near-field adaptive beamforming with distance discrimination," *IEEE Tran. on Audio, Speech, and Language Proc.*, vol. 12, no. 5, pp. 478–488, 2004.
- [7] S. Doclo, S. Gannot, M. Moonen, A. Spriet, S. Haykin, and K. R. Liu, "Acoustic beamforming for hearing aid applications," *Handbook on array processing and sensor networks*, pp. 269–302, 2010.
- [8] H. Cox, R. Zeskind, and M. Owen, "Robust adaptive beamforming," *IEEE Tran. on Acoustics, Speech, and Signal Proc.*, vol. 35, no. 10, pp. 1365–1376, 1987.
- [9] J. Li, P. Stoica, and Z. Wang, "On robust Capon beamforming and diagonal loading," *IEEE Tran. on Signal Proc.*, vol. 51, no. 7, pp. 1702–1715, 2003.
- [10] —, "Doubly constrained robust Capon beamformer," *IEEE Tran. on Signal Proc.*, vol. 52, no. 9, pp. 2407–2423, 2004.
- [11] A. Barnov, V. B. Bracha, S. Markovich-Golan, and S. Gannot, "Spatially robust GSC beamforming with controlled white noise gain," in *Int. Workshop on Acous. Sig. Enhancement (IWAENC)*, 2018, pp. 231–235.
- [12] B. Laufer-Goldshtein, R. Talmon, and S. Gannot, "A study on manifolds of acoustic responses," in *Int. Conf. on Latent Variable Analysis and Sig. Separation*. Springer, 2015, pp. 203–210.
- [13] J. B. Tenenbaum, V. De Silva, and J. C. Langford, "A global geometric framework for nonlinear dimensionality reduction," *Science*, vol. 290, no. 5500, pp. 2319–2323, 2000.
- [14] S. T. Roweis and L. K. Saul, "Nonlinear dimensionality reduction by locally linear embedding," *Science*, vol. 290, no. 5500, pp. 2323–2326, 2000.
- [15] M. Belkin and P. Niyogi, "Laplacian eigenmaps and spectral techniques for embedding and clustering," in *Neural Information Systems Proc. (NIPS)*, vol. 14, no. 14, 2001, pp. 585–591.
- [16] S. Gannot, E. Vincent, S. Markovich-Golan, and A. Ozerov, "A consolidated perspective on multimicrophone speech enhancement and source separation," *IEEE/ACM Tran. on Audio, Speech, and Language Proc.*, vol. 25, no. 4, pp. 692–730, 2017.
- [17] O. Shmaryahu and S. Gannot, "On the importance of acoustic reflections in beamforming," in *International Workshop on Acoustic Signal Enhancement (IWAENC)*, Sep. 2022.
- [18] T. N. Kipf and M. Welling, "Semi-supervised classification with graph convolutional networks," in *International Conference on Learning Representations (ICLR)*, 2022.
- [19] M. Schlichtkrull, T. N. Kipf, P. Bloem, R. Van Den Berg, I. Titov, and M. Welling, "Modeling relational data with graph convolutional networks," in *European Semantic WEB Conference*. Springer, 2018, pp. 593–607.
- [20] S. Zhang, H. Tong, J. Xu, and R. Maciejewski, "Graph convolutional networks: a comprehensive review," *Computational Social Networks*, vol. 6, no. 1, pp. 1–23, 2019.
- [21] P. Veličković, G. Cucurull, A. Casanova, A. Romero, P. Liò, and Y. Bengio, "Graph attention networks," in *International Conference on Learning Representations (ICLR)*, 2018.
- [22] Y. Wang, Y. Sun, Z. Liu, S. E. Sarma, M. M. Bronstein, and J. M. Solomon, "Dynamic graph cnn for learning on point clouds," *ACM Tran. on Graphics*, vol. 38, no. 5, pp. 1–12, 2019.
- [23] J. Zhou, G. Cui, S. Hu, Z. Zhang, C. Yang, Z. Liu, L. Wang, C. Li, and M. Sun, "Graph neural networks: A review of methods and applications," *AI Open*, vol. 1, pp. 57–81, 2020.
- [24] R. Talmon and S. Gannot, "Relative transfer function identification on manifolds for supervised GSC beamformers," in *21st European Signal Proc. Conference (EUSIPCO)*, 2013.
- [25] A. Sofer, T. Kounovský, J. Čmejla, Z. Koldovský, and S. Gannot, "Robust relative transfer function identification on manifolds for speech enhancement," in *29th European Signal Proc. Conference (EUSIPCO)*, 2021, pp. 401–405.
- [26] D. P. Kingma and M. Welling, "Auto-encoding variational bayes," in *Int. Conf. on Learning Representations*, 2014.
- [27] K. Sohn, H. Lee, and X. Yan, "Learning structured output representation using deep conditional generative models," *Advances in neural information Proc. systems*, vol. 28, 2015.
- [28] A. Makhzani, J. Shlens, N. Jaitly, I. Goodfellow, and B. Frey, "Adversarial autoencoders," *arXiv preprint arXiv:1511.05644*, 2015.
- [29] B. Laufer-Goldshtein, R. Talmon, and S. Gannot, "Semi-supervised sound source localization based on manifold regularization," *IEEE/ACM Tran. on Audio, Speech, and Language Proc.*, vol. 24, no. 8, pp. 1393–1407, 2016.
- [30] A. Deleforge and R. Horaud, "2D sound-source localization on the binaural manifold," in *IEEE International Workshop on Machine Learning for Signal Proc. (MLSP)*, 2012.
- [31] B. Laufer-Goldshtein, R. Talmon, and S. Gannot, "Semi-supervised source localization on multiple manifolds with distributed microphones," *IEEE/ACM Tran. on Audio, Speech, and Language Proc.*, vol. 25, no. 7, pp. 1477–1491, 2017.
- [32] A. Deleforge, F. Forbes, and R. Horaud, "Acoustic space learning for sound-source separation and localization on binaural manifolds," *Int. J. of Neural Systems*, vol. 25, no. 1, p. 1440003, 2015.
- [33] A. Brendel, J. Zeitler, and W. Kellermann, "Manifold learning-supported estimation of relative transfer functions for spatial filtering," in *IEEE Inter. Conf. on Acoustics, Speech and Signal Proc. (ICASSP)*, 2022, pp. 8792–8796.
- [34] R. R. Coifman and S. Lafon, "Geometric harmonics: a novel tool for multiscale out-of-sample extension of empirical functions," *Applied and Computational Harmonic Analysis*, vol. 21, no. 1, pp. 31–52, 2006.
- [35] J. Svoboda, J. Masci, F. Monti, M. Bronstein, and L. Guibas, "Peernets: Exploiting peer wisdom against adversarial attacks," in *International Conference on Learning Representations (ICLR)*, 2019.
- [36] F. R. Chung, *Spectral graph theory*. American Mathematical Soc., 1997, vol. 92.
- [37] D. Spielman, "Spectral graph theory," *Combinatorial Scientific Computing*, vol. 18, 2012.
- [38] J. Bruna, W. Zaremba, A. Szlam, and Y. Lecun, "Spectral networks and locally connected networks on graphs," in *International Conference on Learning Representations (ICLR)*, 2014.
- [39] M. Henaff, J. Bruna, and Y. LeCun, "Deep convolutional networks on graph-structured data," *arXiv preprint arXiv:1506.05163*, 2015.
- [40] M. Defferrard, X. Bresson, and P. Vandergheynst, "Convolutional neural networks on graphs with fast localized spectral filtering," *Advances in neural information Proc. systems*, vol. 29, pp. 3844–3852, 2016.
- [41] J. Atwood and D. Towsley, "Diffusion-convolutional neural networks," in *Advances in neural information Proc. systems*, 2016, pp. 1993–2001.
- [42] M. Niepert, M. Ahmed, and K. Kutzkov, "Learning convolutional neural networks for graphs," in *International conference on machine learning (ICML)*, 2016, pp. 2014–2023.
- [43] J. Gilmer, S. S. Schoenholz, P. F. Riley, O. Vinyals, and G. E. Dahl, "Neural message passing for quantum chemistry," in *International conference on machine learning (ICML)*, 2017, pp. 1263–1272.

- [44] W. L. Hamilton, R. Ying, and J. Leskovec, "Inductive representation learning on large graphs," in *Proceedings of the 31st International Conference on Neural Information Proc. Systems (NeurIPS)*, 2017, pp. 1025–1035.
- [45] F. Monti, D. Boscaini, J. Masci, E. Rodola, J. Svoboda, and M. M. Bronstein, "Geometric deep learning on graphs and manifolds using mixture model cnns," in *IEEE conference on Computer Vision and Pattern Recognition (CVPR)*, 2017, pp. 5115–5124.
- [46] W. Cao, Z. Yan, Z. He, and Z. He, "A comprehensive survey on geometric deep learning," *IEEE Access*, vol. 8, pp. 35 929–35 949, 2020.
- [47] U. Alon and E. Yahav, "On the bottleneck of graph neural networks and its practical implications," in *International Conference on Learning Representations (ICLR)*, 2021.
- [48] S. Markovich, S. Gannot, and I. Cohen, "Multichannel eigenspace beamforming in a reverberant noisy environment with multiple interfering speech signals," *IEEE Tran. on Audio, Speech, and Language Proc.*, vol. 17, no. 6, pp. 1071–1086, 2009.
- [49] S. Markovich-Golan and S. Gannot, "Performance analysis of the covariance subtraction method for relative transfer function estimation and comparison to the covariance whitening method," in *IEEE Inter. Conf. on Acoustics, Speech and Signal Proc. (ICASSP)*, 2015, pp. 544–548.
- [50] J. Čmejla, T. Kounovský, S. Gannot, Z. Koldovský, and P. Tandeitnik, "MIRaGe: multichannel database of room impulse responses measured on high-resolution cube-shaped grid," in *28th European Signal Proc. Conference (EUSIPCO)*, 2021, pp. 56–60.
- [51] G. Li, M. Muller, A. Thabet, and B. Ghanem, "DeepGCNs: Can GCNs go as deep as CNNs?" in *Proceedings of the IEEE/CVF International Conference on Computer Vision (ICCV)*, 2019, pp. 9267–9276.
- [52] Q. Li, Z. Han, and X.-M. Wu, "Deeper insights into graph convolutional networks for semi-supervised learning," in *32nd AAAI Conference on Artificial Intelligence*, 2018.
- [53] R. Talmon and S. Gannot, "Relative transfer function identification on manifolds for supervised GSC beamformers," in *21st Eurasip Signal Proc. Conference (EUSIPCO)*, 2013.
- [54] J. Le Roux, S. Wisdom, H. Erdogan, and J. R. Hershey, "SDR–half-baked or well done?" in *IEEE Inter. Conf. on Acoustics, Speech and Signal Proc. (ICASSP)*, 2019, pp. 626–630.
- [55] C. H. Taal, R. C. Hendriks, R. Heusdens, and J. Jensen, "An algorithm for intelligibility prediction of time-frequency weighted noisy speech," *IEEE Tran. on Audio, Speech, and Language Proc.*, vol. 19, no. 7, pp. 2125–2136, 2011.
- [56] C. K. Reddy, V. Gopal, and R. Cutler, "DNSMOS P. 835: A non-intrusive perceptual objective speech quality metric to evaluate noise suppressors," in *IEEE Inter. Conf. on Acoustics, Speech and Signal Proc. (ICASSP)*, 2022, pp. 886–890.